RSC Advances

PAPER

View Article Online
View Journal | View Issue

Cite this: *RSC Adv.*, 2022, **12**, 16570

Novel near-infrared reflective black inorganic pigment based on cerium vanadate

Takuro Moriomoto,[a] Ryohei Oka, *[b] Kohei Minagawa[a] and Toshiyuki Masui *[cd]

Received 18th April 2022
Accepted 25th May 2022

DOI: 10.1039/d2ra02483g

rsc.li/rsc-advances

Gd^{3+}-doped cerium vanadates, $Ce_{1-x}Gd_xVO_4$ ($0 \leq x \leq 0.30$), were synthesized as near-infrared (NIR) reflective black pigments by a conventional solid-state reaction method. Crystal structure, particle size, optical properties, and color of the samples were characterized. The $Ce_{1-x}Gd_xVO_4$ ($0 \leq x \leq 0.30$) samples were obtained in a single-phase form and the lattice volume decreased with increasing Gd^{3+} concentration. Optical absorption below 630 nm was observed in all samples, which corresponded to the charge-transfer transition between Ce_{4f} and V_{3d} orbitals. The absorption spectrum of $Ce_{1-x}Gd_xVO_4$ was shifted to the longer wavelength side as the Gd^{3+} content increased, because of the increase in the crystal field around V^{5+} due to the lattice shrinkage. As a result, the sample color gradually changed from dark brown to black with increasing Gd^{3+} content. Among the samples synthesized in this study, $Ce_{0.80}Gd_{0.20}VO_4$ absorbed visible light with wavelengths shorter than 650 nm and exhibited the darkest color. Furthermore, this black pigment showed a sufficient NIR reflectance value ($R = 66.3\%$), which was higher than those of the commercially available products ($R < 50\%$).

Introduction

The urban heat-island effect gives rise to the ambient temperature in an urban area being higher than that in the surrounding countryside. This phenomenon often adversely affects the habitability of many cities, including the high-power consumption of air conditioners, poor air quality, and human health in the summer.[1] Natural sunlight consists of 5% ultraviolet light (UV; 280–400 nm), 43% visible light (Vis; 400–700 nm), and 52% near-infrared light (NIR; 700–2500 nm).[2] The photon energy obtained by absorbing light is converted into vibration energy and finally into thermal energy. In addition, NIR light in the wavelength range of 700 to 1300 nm plays the most important role in heat generation.[3] Therefore, in order to mitigate heat storage, it is desirable for the material to reflect NIR light in this region, and pigments of various colors that reflect NIR light have been reported.[4–18]

The NIR reflection properties of various color pigments (white, yellow, blue, *etc.*) are generally superior to those of black pigments, because these pigments tend to reflect NIR light as well as visible light.[19,20] Common black pigments such as carbon black basically absorb not only visible light but also NIR light to store heat. Generally, they are painted on roads and exterior walls, so in urban areas where the proportion of roads and exterior walls is higher than that of green areas, the temperature rises, and the artificial heat exhausted by air conditioning increases.[21] The heat island effect is a serious problem in the world. By using NIR reflective black pigment on the road surface and the wall of the building, it can be expected to alleviate the phenomenon. Several compounds such as $(Fe, Cr)_2O_3$ and Fe_2TiO_4 have been reported as NIR-reflective black pigments.[4,22] However, $(Fe, Cr)_2O_3$ contains toxic chromium, and the NIR-reflective properties of both materials are not sufficient.

This study focused on cerium vanadate ($CeVO_4$) as the host material for environmentally friendly NIR-reflective black pigments composed of only low toxic elements. It has been reported that $CeVO_4$ shows optical absorption due to a Ce_{4f}–V_{3d} charge transfer transition and its optical band gap energy is 1.8 eV.[23,24] Therefore, this vanadate compound should exhibit a dark brown color and reflect NIR light. The wavelength of the optical absorption caused by the Ce_{4f}–V_{3d} charge transfer transition can be controlled by adjusting the crystal field strength around V^{5+}, because the split width of the V_{3d} orbitals corresponds to the crystal field strength, which is enhanced by the lattice contraction. Since the absorption wavelength depends on the energy difference between the Ce_{4f} and the V_{3d} orbitals, the optical absorption wavelength shifts to the longer wavelength side when smaller ions are doped into the Ce^{3+} site.

[a]*Department of Engineering, Graduate School of Sustainability Science, Tottori University, 4-101, Koyama-cho Minami, Tottori 680-8552, Japan*

[b]*Field of Advanced Ceramics, Department of Life Science and Applied Chemistry, Nagoya Institute of Technology, Gokiso, Showa, Nagoya, 466-8555, Japan. E-mail: oka.ryohei@nitech.ac.jp; Tel: +81-52-735-5365*

[c]*Faculty of Engineering, Tottori University, 4-101, Koyama-cho Minami, Tottori 680-8552, Japan*

[d]*Canter for Research on Green Sustainable Chemistry, Tottori University, 4-101, Koyama-cho Minami, Tottori 680-8552, Japan. E-mail: masui@tottori-u.ac.jp; Fax: +81-857-31-5264; Tel: +81-857-31-5264*

As a dopant to modify the crystal field strength, Gd^{3+} (ionic radius: 0.1053 nm),[25] which is smaller than Ce^{3+} (ionic radius: 0.1143 nm),[25] was selected. When Gd^{3+} ions are doped into the Ce^{3+} site, the split width of the V_{3d} orbital should be widened due to lattice shrinkage. The color of the material is expected to change from dark brown to black due to the decrease in the energy between the Ce_{4f} and the V_{3d} orbitals. Therefore, $Ce_{1-x}Gd_xVO_4$ ($0 \leq x \leq 0.30$) solid solutions were synthesized in this study. Their NIR reflection and color properties were characterized, and the composition was optimized to satisfy both sufficient blackness and high NIR reflectance.

Experimental

Materials and methods

The $Ce_{1-x}Gd_xVO_4$ ($0 \leq x \leq 0.30$) powder samples were synthesized by a conventional solid-state reaction method. Stoichiometric amounts of CeO_2 (FUJIFILM Wako Pure Chemical Industries, Ltd., 99.5%), V_2O_5 (FUJIFILM Wako Pure Chemical Industries, Ltd., 99.0%), and Gd_2O_3 (Shin-Etsu Chemical Co., Ltd., 99.9%) were mixed in an agate mortar. The mixtures were calcined in an alumina crucible at 900 °C for 6 h in an air atmosphere. Finally, the samples were ground in an agate mortar before characterization.

Characterization

The powder samples obtained were characterized by the following methods. The chemical composition of the samples analyzed by X-ray fluorescence spectroscopy (XRF; Rigaku, ZSX Primus) were in good agreement with the nominal stoichiometric compositions of the starting mixtures. The crystal structure was identified by X-ray powder diffraction (XRD; Rigaku, Ultima IV) with Cu-Kα radiation (40 kV and 40 mA). The sampling width and the scan speed were 0.02° and 6 min^{-1}, respectively. The lattice volume was calculated with the CellCalc Ver. 2.20 software from the XRD peak angles refined using α-Al_2O_3 as a standard. The morphology of the $Ce_{1-x}Gd_xVO_4$ ($x = 0$, 0.10, 0.20 and 0.30) particles was investigated using a field-emission-type scanning electron microscope (FE-SEM; JEOL, JSM-6701F).

The optical reflectance spectra were measured using an ultraviolet-visible-near-infrared (UV-Vis-NIR) spectrometer (JASCO, V-770 with an integrating sphere attachment). Barium sulphate ($BaSO_4$) and polytetrafluoroethylene (PTFE) powders were used as reference samples in the visible and NIR light regions, respectively. NIR solar reflectance (R) was calculated according to the American Society for Testing and Materials (ASTM) Standard G173-03 and estimated by the following formula:

$$R = \frac{\int_{700}^{2500} r(\lambda) i(\lambda) \mathrm{d}\lambda}{\int_{700}^{2500} i(\lambda) \mathrm{d}\lambda}$$

where $r(\lambda)$ is the spectral reflectance obtained from the experiment and $i(\lambda)$ is the standard solar spectrum (W m^{-2} nm^{-1}). The NIR reflectance value (R) was expressed as the integral of the product of the observed spectral reflectance and the solar irradiance divided by the integral of the solar irradiance, both integrated in the range of 700 to 2500 nm. The band gap energies of the samples were calculated from the absorption edge of the absorbance spectrum represented by the Kubelka–Munk function, $f(R) = (1 - R)^2/2R$, where R is reflectance.[26] The color property was evaluated in terms of the Commission Internationale de l'Éclairage (CIE) $L^*a^*b^*C$ system using a colorimeter (Konica-Minolta, CR-400). The L^* parameter indicates the brightness or darkness of a color relative to the neutral gray scale, and the a^* (the red-green axis) and the b^* (the yellow-blue axis) parameters represent the color quantitatively. The chroma parameter (C) represents the color saturation of the pigments and is calculated according to the following formula: $C = [(a^*)^2 + (b^*)^2]^{1/2}$.

Results and discussion

X-ray powder diffraction (XRD) and field-emission-type scanning electron microscopic (SEM) image

Fig. 1 shows the XRD patterns of the $Ce_{1-x}Gd_xVO_4$ ($0 \leq x \leq 0.30$) samples. It has been reported that $CeVO_4$ has tetragonal[27,28] and monoclinic structures.[28–30] In all samples, the diffraction pattern was indexed to that of the tetragonal $CeVO_4$ phase and obtained in a single-phase form. The lattice volumes of the $Ce_{1-x}Gd_xVO_4$ ($0 \leq x \leq 0.30$) samples are listed in Table 1. The lattice volume monotonically decreased as the Gd^{3+} concentration increased. These results indicated that Ce^{3+} ions (0.1143 nm)[25] in the $CeVO_4$ lattice were partially substituted with smaller Gd^{3+} ions (0.1053 nm)[25] and the $Ce_{1-x}Gd_xVO_4$ ($0 \leq x \leq 0.30$) solid solutions were successfully synthesized in a single-phase form.

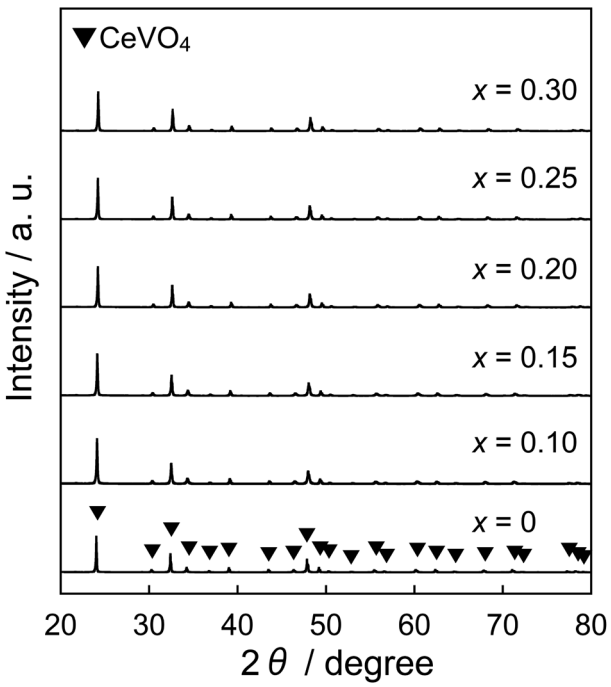

Fig. 1 XRD patterns of the $Ce_{1-x}Gd_xVO_4$ ($0 \leq x \leq 0.30$) samples.

Table 1 Lattice volumes of $Ce_{1-x}Gd_xVO_4$ ($0 \leq x \leq 0.30$)

x	Lattice volume/nm^3
0	0.3551
0.10	0.3529
0.15	0.3514
0.20	0.3501
0.25	0.3491
0.30	0.3478

Fig. 2 shows the FE-SEM images and particle size distributions of the $Ce_{1-x}Gd_xVO_4$ ($0 \leq x \leq 0.30$) samples. The average particle size increased with increasing the Gd^{3+} concentration; the size increased from 1.99 mm ($x = 0$) to 3.49 mm ($x = 0.30$). This particle growth was promoted by the Gd^{3+} doping, because the melting point of $GdVO_4$ (1800 °C)[31] is lower than that of $CeVO_4$ (1832 °C).[32]

Reflectance spectra

The UV-Vis-NIR reflectance spectra of the $Ce_{1-x}Gd_xVO_4$ ($0 \leq x \leq 0.30$) samples are shown in Fig. 3(a). An enlarged view of the reflectance spectra in the visible light region (300–750 nm) is also depicted in Fig. 3(b). All samples were found to strongly absorb visible light with wavelengths shorter than 650 nm, and this optical absorption was attributed to the Ce_{4f}–V_{3d} charge transfer transition.[23] Since the crystal field energy around V^{5+} was increased by the lattice contraction, the spectral curve was shifted to the longer wavelength side by the Gd^{3+} doping. Actually, the band gap energy was decreased by the Gd^{3+} doping, as shown later in Table 2. As a result, the color of the sample gradually changed from reddish brown to black as the Gd^{3+} content increased.

In the range of x from 0 to 0.20, the absorption wavelength shifted to the longer wavelength side with increasing the amount of Gd^{3+}. Since the ionic radius of Gd^{3+} is smaller than that of Ce^{3+}, partial replacement of Ce^{3+} with Gd^{3+} causes the crystal lattice to contract and the crystal field energy near V^{5+} to increase. This red shift of the spectral curve was due to a decrease in the transition energy between the Ce_{4f} and the V_{3d} orbitals, caused by an increase in the split width of the V_{3d} orbitals. In the x region of $x \geq 0.20$, on the other hand, the

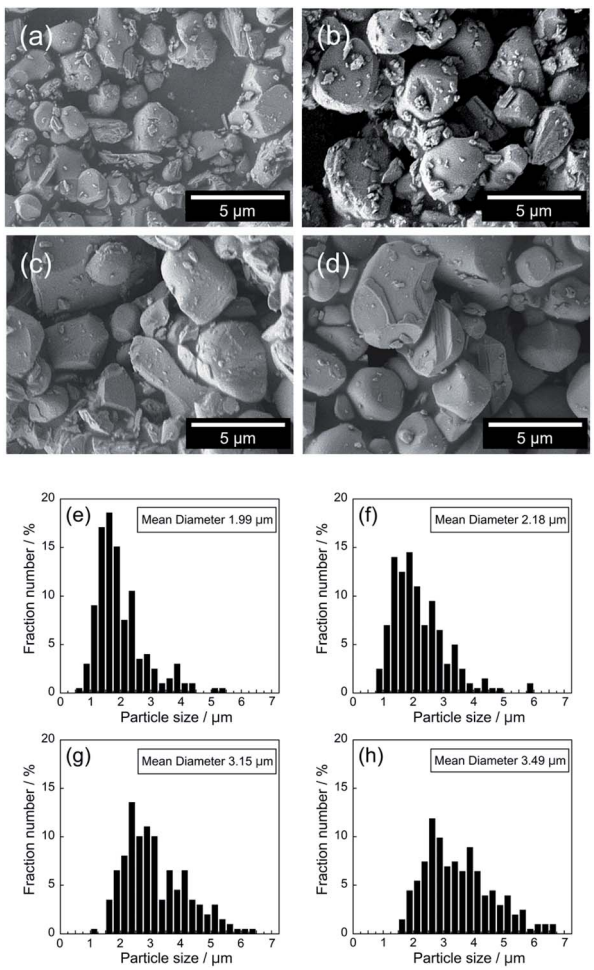

Fig. 2 FE-SEM images and particle size distributions of $Ce_{1-x}Gd_xVO_4$; $x = 0$ (a and e), $x = 0.10$ (b and f), $x = 0.20$ (c and g), and $x = 0.30$ (d and h).

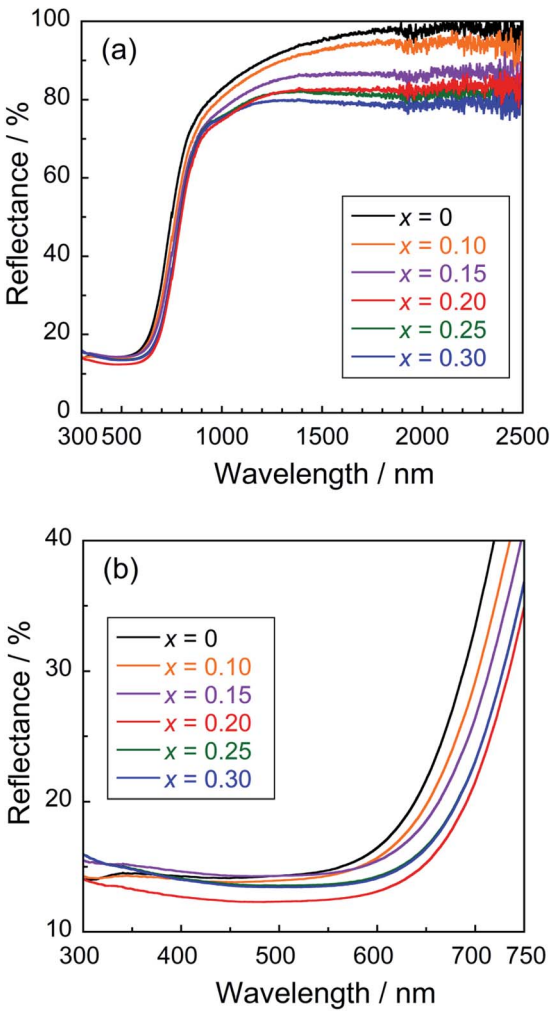

Fig. 3 Reflectance spectra of the UV-Vis-NIR (a) and UV-Vis (b) regions of the $Ce_{1-x}Gd_xVO_4$ ($0 \leq x \leq 0.30$) samples.

Table 2 Color coordinates, bandgap energies (E_g) and NIR solar reflectance (R) of the $Ce_{1-x}Gd_xVO_4$ ($0 \leq x \leq 0.30$) powder samples

x	L^*	a^*	b^*	C	E_g/eV	R/%
0	26.8	+11.1	+6.62	12.9	1.69	77.5
0.10	27.3	+8.57	+5.14	9.99	1.67	74.1
0.15	25.1	+6.99	+3.72	7.92	1.63	70.0
0.20	22.2	+5.71	+2.77	6.35	1.60	66.3
0.25	23.2	+6.14	+3.24	6.94	1.62	67.0
0.30	23.1	+6.17	+3.18	6.99	1.62	66.0

spectral curve shifted to the shorter wavelength side as the Gd^{3+} content increased. This blue shift was due to the narrowing of the energy band of the Ce_{4f} orbitals due to the decrease in the Ce^{3+} concentration, leading to an increase in the Ce_{4f}–V_{3d} charge transfer energy. In other words, there is a trade-off relationship between the increase in the splitting width of the V_{3d} orbitals and narrowing of the Ce_{4f} orbitals. The boundary between the x regions, where the former and latter effects were dominant, was approximately $x = 0.20$.

When Gd^{3+} was doped, the NIR reflectivity of the sample decreased. Based on the Mie scattering theory,[33] light scattering capacity is generally maximized when the particle size is approximately equal to the wavelength of the corresponding light. As already shown in Fig. 2, the average particle size of the sample increased from 1.99 to 3.49 μm with increasing the Gd^{3+} concentration. Therefore, the decrease in the NIR reflectivity was caused by an increase in the number of particles that were too large in size compared to the wavelength of NIR light (700–2500 nm).[34]

Chromatic properties and NIR solar reflectance

The $L^*a^*b^*C$ color coordinate data, bandgap energies (E_g) and NIR solar reflectance (R) of the $Ce_{1-x}Gd_xVO_4$ ($0 \leq x \leq 0.30$) powder samples are summarized in Table 2. The photographs of them are also displayed in Fig. 4. In the x region of $x \leq 0.20$, the brightness (L^*), redness (a^*), yellowness (b^*) and chroma (C) values were decreased by doping with Gd^{3+}. When $0.25 \leq x$, on the other hand, the L^*, a^*, b^*, and C values of $Ce_{1-x}Gd_xVO_4$ ($0.25 \leq x$) were almost the same as those of the $x = 0.20$ sample. These results are consistent with the reflection behavior in the red light (600–750 nm) region shown in Fig. 3. The sample color gradually changed from reddish brown to black with increasing the Gd^{3+} content. The darkest black was obtained with $Ce_{0.80}Gd_{0.20}VO_4$ among all samples. As mentioned in Fig. 3(a), the optical reflection in the NIR light region (700–2500 nm) was reduced by the partial substitution of Ce^{3+} with Gd^{3+}, resulting in the decrease in the R value. However, the $Ce_{0.80}Gd_{0.20}VO_4$ sample, which exhibited the darkest black of all samples, showed a sufficient high R value (66.3%). From these results above, $Ce_{0.80}Gd_{0.20}VO_4$ is considered the best black pigment with good NIR-reflective property.

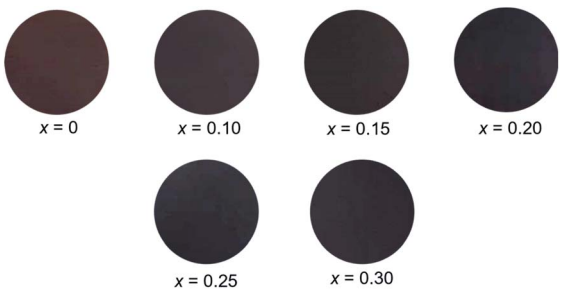

Fig. 4 Photographs of the $Ce_{1-x}Gd_xVO_4$ ($0 \leq x \leq 0.30$) pellets made from the powder samples.

Table 3 Color coordinates of $Ce_{0.80}Gd_{0.20}VO_4$ before and after chemical stability test

Treatment	L^*	a^*	b^*	C	R/%
As synthesized	22.2	+5.71	+2.77	6.35	66.3
4% CH_3COOH	21.3	+5.31	+2.62	5.92	69.1
4% NH_4HCO_3	21.4	+5.38	+2.78	6.06	72.3

Chemical stability tests

The chemical stability of the $Ce_{0.80}Gd_{0.20}VO_4$ pigment was evaluated using the powder sample. The acid/base resistance of the $Ce_{0.80}Gd_{0.20}VO_4$ pigment was tested in 4% CH_3COOH and 4% NH_4HCO_3 aqueous solutions, and the pigment was soaked in the acid solution and the base solution, respectively. After allowing them to stand at room temperature for 2 h, the pigments were washed with deionized water and ethanol and then dried at ambient temperature.

The chromatic coordinate data of the samples after the chemical stability test are summarized in Table 3. The color was almost unchanged after the leaching test in the acid and the base solutions. Therefore, the $Ce_{0.80}Gd_{0.20}VO_4$ pigment has chemical stability.

Comparison with commercially available pigments

The UV-Vis-NIR diffuse reflectance spectrum and the color parameters for the optimized $Ce_{0.80}Gd_{0.20}VO_4$ pigment were

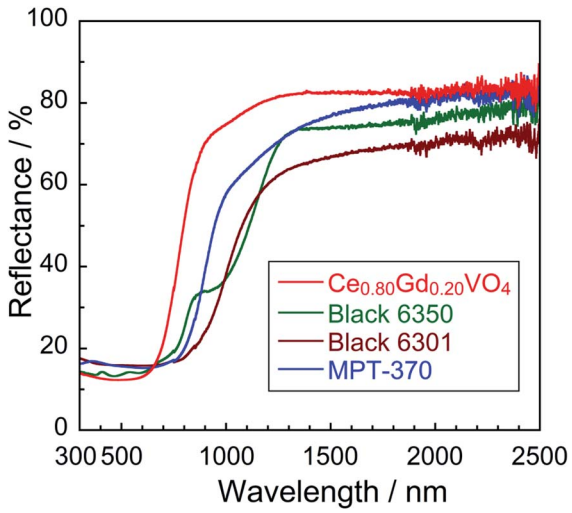

Fig. 5 UV-Vis-NIR reflectance spectra of various black pigments.

Table 4 Color coordinates and NIR solar reflectance (R) of various black pigments

Pigment	L^*	a^*	b^*	C	R/%
$Ce_{0.80}Gd_{0.20}VO_4$	22.2	+5.71	+2.77	6.35	66.3
Black 6350	27.0	+0.78	+3.53	3.62	44.7
Black 6301	25.0	+0.42	+0.97	1.06	40.1
MPT-370	25.7	+0.59	−0.48	6.35	49.0

Fig. 6 Photographs of $Ce_{0.80}Gd_{0.20}VO_4$ (a), Black 6350 (b), Black 6301 (c), and MPT-370 (d) pellets made from the powder samples.

compared with those of several commercially available NIR-reflective black pigments such as Black 6350 (iron and chromium oxide; Asahi Kasei), Black 6301 (manganese and bismuth oxide, Asahi Kasei), and MPT-370 (calcium, manganese, and titanium oxide, Ishihara Sangyo). The UV-Vis-NIR results are shown in Fig. 5 and the color parameters are summarized in Table 4. The photographs of these pigments are also demonstrated in Fig. 6. As evidenced from these results, the present $Ce_{0.80}Gd_{0.20}VO_4$ pigment showed higher reflectance in the NIR wavelength region and higher R values than those of the commercially available pigments. Therefore, we can conclude that $Ce_{0.80}Gd_{0.20}VO_4$ is a novel black pigment with sufficient blackness and NIR-reflective property.

Conclusions

The $Ce_{1-x}Gd_xVO_4$ ($0 \leq x \leq 0.30$) solid solutions were synthesized by a conventional solid-state reaction method with the aim of developing a new NIR-reflective black pigment. In the samples with the x range of 0 to 0.20, the spectral curve shifted to the longer wavelength side because the energy gap between the Ce_{4f} and the V_{3d} orbitals decreased as the crystal field energy around V^{5+} increased due to the lattice shrinkage. As a result, the color of the sample gradually changed from reddish brown to black. Both adequate blackness and high NIR solar reflectance (R) were obtained at $Ce_{0.80}Gd_{0.20}VO_4$. The R value for this sample was 66.3% and the $L^*a^*b^*C$ color parameters were $L^* = 22.2$, $a^* = +5.71$, $b^* = +2.77$, and $C = 6.35$, respectively. In particular, the R value was significantly higher than those of the conventional commercially available black pigments ($R < 50\%$). $Ce_{0.80}Gd_{0.20}VO_4$ has both sufficient blackness and NIR-reflective property, which could make this pigment an effective alternative to the conventional black pigments for thermal shielding.

Conflicts of interest

There are no conflicts to declare.

Acknowledgements

This work was supported by JSPS KAKENHI (Grant Numbers JP19K05668 and JP20H02439).

References

1 A. Mohajerani, J. Bakaric and T. Jeffrey-Bailey, *J. Environ. Manage.*, 2017, **197**, 522.
2 L. Liu, A. Han, M. Ye and W. Feng, *Sol. Energy*, 2015, **113**, 48.
3 B. Kaur, N. Quazi, I. Ivanov and S. N. Bhattacharya, *Dyes Pigm.*, 2012, **92**, 1108.
4 R. Levinson, P. Berdahl and H. Akbari, *Sol. Energy Mater. Sol. Cells*, 2005, **89**, 351.
5 P. Jeevanandam, R. S. Mulukutla, M. Phillips, S. Chaudhuri, L. E. Erickson and K. J. Klabunde, *J. Phys. Chem. C*, 2007, **111**, 1912.
6 L. S. Kumarai, P. P. Rao, A. N. P. Radhakrishnan, V. James, S. Sameera and P. Koshy, *Sol. Energy Mater. Sol. Cells*, 2013, **112**, 134.
7 T. R. Aju Thara, P. P. Rao, S. Divya, A. K. V. Raj and T. S. Sreena, *ACS Sustainable Chem. Eng.*, 2017, **5**, 5118.
8 M. Zhao, A. Han, M. Ye and T. Wu, *Sol. Energy*, 2013, **97**, 350.
9 V. Elakkiya and S. Sumathi, *Mater. Lett.*, 2020, **263**, 127246.
10 A. K. V. Raj, P. P. Rao, S. Divya and T. R. Ajuthara, *Powder Technol.*, 2017, **311**, 52; P. Meenakshi and M. Selvaraj, *Sol. Energy Mater. Sol. Cells*, 2018, **174**, 530.
11 P. Meenakshi and M. Selvaraj, *Sol. Energy Mater. Sol. Cells*, 2018, **174**, 530.
12 B. Huang, Y. Xiao, H. Zhou, J. Chen and X. Sun, *ACS Sustainable Chem. Eng.*, 2018, **6**, 10735.
13 A. E. Smith, M. C. Comstock and M. A. Subramanian, *Dyes Pigm.*, 2016, **133**, 214.
14 S. Jose and M. L. Reddy, *Dyes Pigm.*, 2013, **98**, 540.
15 R. Ianoș, E. Muntean, C. Păcurariu, R. Lazău, C. Bandas and G. Delinescu, *Dyes Pigm.*, 2017, **142**, 24.
16 D. Saraswathy, P. P. Rao, A. K. V. Raj and T. R. Ajuthara, *Dyes Pigm.*, 2017, **142**, 472.
17 X. Zhao, Y. Zhang, Y. Huang, H. Gong and J. Zhao, *Dyes Pigm.*, 2015, **116**, 119.
18 S. Jose, A. Prakash, S. Laha, S. Natarajan and M. L. Reddy, *Dyes Pigm.*, 2014, **107**, 118.
19 R. Levinson, P. Berdahl, H. Akbari, W. Miller, I. Joedicke, J. Reilly, Y. Suzuki and M. Vondran, *Sol. Energy Mater. Sol. Cells*, 2007, **91**, 304.
20 R. Levinson, H. Akbaria and J. C. Reilly, *Build. Environ.*, 2007, **42**, 2591.
21 A. Mohajerani, J. Bakaric and T. Jeffrey-Bailey, *J. Environ. Manage.*, 2017, **197**, 522.
22 E. B. Faulkner and R. J. Schwartz, *High Performance Pigments*, 2nd edn, Wiley-VCH, 2009.
23 M. R. Dolgos, A. M. Paraskos, M. W. Stoltzfus, S. C. Yarnell and P. M. Woodward, *J. Solid State Chem.*, 2009, **182**, 1964.
24 M. Oshikiri, J. Ye and M. Boero, *J. Phys. Chem. C*, 2014, **118**, 8331.
25 R. D. Shannon, *Acta Crystallogr., Sect. A: Cryst. Phys., Diffr., Theor. Gen. Crystallogr.*, 1976, **32**, 751.

26 P. Kubelka and F. Munk, *Z. Tech. Phys.*, 1931, **12**, 593.
27 C. T. G. Petit, R. Lan, P. I. Cowin and S. Tao, *J. Solid State Chem.*, 2010, **183**, 1231.
28 A. B. Garg, K. V. Shanavas, B. N. Wani and S. M. Sharma, *J. Solid State Chem.*, 2013, **203**, 273.
29 K.-J. Range, H. Meister and U. Klement, *Z. Naturforsch., B: J. Chem. Sci.*, 1990, **45**, 598.
30 M. Yoshimura and T. Sata, *Bull. Chem. Soc. Jpn.*, 1969, **42**, 3195.
31 G. A. Rykova, V. M. Skorikov, Yu. M. Baryshnikov and G. G. Yagol'nikov, *Russ. J. Inorg. Chem.*, 1976, **21**, 1698.
32 L. S. O'Bannon, *Dictionary of Ceramic Science and Engineering*, Plenum Press, New York, 1984.
33 G. Mie, *Ann. Phys.*, 1908, **25**, 377.
34 J. Song, J. Qin, J. Qu, Z. Song, W. Zhang, X. Xue, Y. Shi, T. Zhang, W. Ji, R. Zhang, H. Zhang, Z. Zhang and X. Wu, *Sol. Energy Mater. Sol. Cells*, 2014, **130**, 42.